Modeling and Simulation of Macrosegregation Induced by Thermomechanical Deformation in Steels

Ali SAAD

December 2014

Contents

Todo list

Introduction

Metallurgical processes have known a great evolution during the last 60 years. The advancement is attributed to research disciplines, like physical metallurgy, which investigated a great deal of solidification-related phenomena. Nowadays, metallurgists and physicists seek to understand deeper the connection between the different scales involved. From the nucleation theory to the mechanical behavior of metals, an chain of intricate phenomena occur in a such a way to create defects in the final product. This has been seen in casting processes like continuous casting and ingot casting. Suface and volume porosity, hot tearing and composition heterogeneities are known defects to the casting community. As far as the current project is concerned, the last defect, widely known as macrosegregation, is the subject of our interest.

Defects

> Worth checking notes from the Ecole Thématique CNRS oléron (Check Mail Draft)

- Hot tearing

- Porosity

- Freckles

- Macrosegregation

Industrial Worries

Production

- Talk about total steel production, variations over the last few decades

- Quality constraints for many applications that require steel like construction, nuclear engines ?

- Difficulties to meet these constraints and what are the present solutions

Research and Simulation

- Need for software handling multicomponent alloys

- Need for software handling finite diffusion in the solid

- Need for realistic alloy properties (not only constants)

- Need for handling moulds along with volume change (creating thermal resistances)

Worth discussing Isabelle Poitraut and David Cardianaux - and Claudine Allentin (respo comm Arcelor Dunkerque, search for mail)

CCEMLCC contribution

- some words about this ESA project

- in what ways does this project tries to alleviate the aforementionned problems ?

- academic and industrial partners and how does each of them contribute actually

- mention *Thercast* as the final developped code destination ?

Chapter 1

Modelling Review

Contents

In this chapter the following points are discussed

- what does a typical solidifications problem consist of ? heat - fluid - solid - chemical species

- what are the modeling scales of these physics ? direct (micro: phase field / macro: CA) and indirect (micro Nancy models / macro: current FE model)

  > Maybe worth showing the 2x2 table that CAG showed at the ICASP conference ?

- Overview of these models ??

- Presence of AIR requires a new problem definition : Lagrangian or Eulerian framework

1.1   Standard FE model

A section presenting the main FE equations along with their weak formulations that will be solved in the metal being a single domain. I call it "standard" because it doesnt contain anything about levelsets, compressibility, ...

- Energy (chapter 1)

- Species mass (voller prakash)

  > should I mention the tabulation approach that I couldnt finalize because of the equality between w and wl in liquid phase ?

- Fluid mechanics (vms: darcy model with boussinesq)

> talking about Eulerian approach Air Metal will be presented in the next chapters, it should be the biblio section of another chapter

1.2   Biblio test

[**?**] are going to appear in the paper

Chapter 2

Energy Balance: temperature solver with thermodynamic tabulations

Contents

> TODO: replace wt pct by the macro bin or tern

> TODO: correct equations references prefix after replacing autoref by eqref

When we speak about macrosegregation in solidification, we have to remember that the problem is one that involves phase change.

2.1   State of the art

- Use of enthalpy resolution in the majority of works

- motivation and advantages of TvsH without talking about resolution time

- use article's introduction to fill this section (or improvise new things)

2.2   Thermodynamic considerations

> this section should be revised for missing symbols, equations and figures from the corresponding article

2.2.1   Volume averaging

A volume averaging technique was suggested to deal with the presence of multiple phases [?]. It locally considers a Representative Volume Element (RVE) that contains a single or several phases (these are not necessarily in thermodynamic equilibrium) at a mesoscopic scale. We represent, for each unknown ψ, an intrinsic volume average, $\langle\psi\rangle^\phi$ (also denoted $\langle\psi^\phi\rangle^\phi$ in the literature), corresponding to a phase ϕ. The volume average $\langle\psi\rangle$ for this unknown in the RVE, hence averaged over all the present phases writes:

$$\langle\psi\rangle = \sum_\phi g^\phi \langle\psi\rangle^\phi \tag{2.1}$$

where g^ϕ denotes the volume fraction of phase ϕ in the RVE. It should be emphasized that the averaging technique applies to virtually all thermodynamic variables (enthalpy, density …). Among these variables, the temperature is also considered to be uniform in the RVE. Applying the volume averaging technique to the energy conservation principle along with interfacial balances between the phases, results in the following averaged equation [?]:

$$\frac{\partial\langle\rho h\rangle}{\partial t} + \vec{\nabla}\cdot\langle\rho h\vec{v}\rangle = \vec{\nabla}\cdot\left(\langle\kappa\rangle\vec{\nabla}T\right) + \langle\dot{Q}_V\rangle \tag{2.2}$$

where ρ stands for the density, h the mass enthalpy, $\vec{v}$ the velocity field, κ the thermal conductivity, T the temperature and $\dot{Q}_V$ a possible volume heat source. (2.2) is the standard averaged form of the energy conservation equation used in non-stationary phase change problems.

> I could elaborate more in this paragraph by showing the possible equations for the explicit formulation and maybe a figure to show the AlSi7 computation that i did with a v small time step

Once the variational form has been discretized in space and time, two possible resolution schemes emerge: the first is an explicit forward Euler scheme which gives rise to a linear equation where the temperature is known at time t, T^t. This requires very small time steps in the current context, which limits the solver's usability at the scale of industrial applications. The second scheme is the backward Euler or full implicit discretization where terms are function of $T^{t+\Delta t}$. It leads to a nonlinear equation with 2 interdependent unknowns, $\langle \rho h \rangle^{t+\Delta t}$ and $T^{t+\Delta t}$. It is clear that the nature of the temperature-enthalpy relationship plays a central role when formulating the resolution strategy of this nonlinear equation. Generally, it is admitted that, depending on the resolution strategy, it is necessary to express enthalpy as a function of temperature or vice-versa, together with associated partial derivatives, $\frac{d\langle \rho h \rangle}{dT}$ or $\frac{dT}{d\langle \rho h \rangle}$.

2.2.2 The temperature-enthalpy relationship

In solidification problems, additional variables are involved in (2.1) and (2.2), like the transformation path that defines the history of the phase fractions, as well as the average chemical composition $\langle w_i \rangle$, i being the index of the chemical species (only the solutes are considered). The temperature-enthalpy relation averaged over the phases in a given RVE writes:

$$\langle \rho h \rangle = \sum_{\phi} g^{\phi}_{(T,\langle w_i \rangle...)} \rho^{\phi}_{(T,\langle w_i \rangle^{\phi}...)} h^{\phi}_{(T,\langle w_i \rangle^{\phi}...)} \tag{2.3}$$

Note that the volume average enthalpy is approximated by the product $\langle \rho h \rangle^{\phi} = \langle \rho \rangle^{\phi} \langle h \rangle^{\phi}$ in the current work. As stated in the introduction, it becomes clear from (2.3) that phase properties, i.e. average phase density, , ρ^{ϕ} and enthalpy, h^{ϕ}, are temperature and composition dependent. This equation is the key to convert the average volume enthalpy to temperature (through a procedure named H2T) or vice-versa (T2H). The values of the different phase fractions g^{ϕ} (solidification path) and phase enthalpies $\langle \rho h \rangle^{\phi}$ are thus needed to close the relation.

2.2.3 Tabulation of properties

The complexity of performing a thermodynamic conversion is directly linked to the simplicity of determining the alloy properties, namely the phase fractions and phase enthalpies. In the case of binary alloys and with several assumptions with respect to the system (e.g., linear monovariant temperature composition relationships, constant heat capacity of phases and constant latent heat of transformations, equilibrium approximations between phases) analytical calculations are often used to determine the properties. Nevertheless, analytical relations are more complex or even impossible to derive in the case of multicomponent alloys (i>1). To overcome this problem, one can resort to thermodynamic databases and phase equilibrium calculations to tabulate the transformation paths and the phase enthalpies for a given range of temperatures and average compositions. It is a handy solution for two main reasons: first, the conversion is merely a binary search in a table; secondly, it is a simple solution for coupling with macrosegregation. In this way, phase fractions g^{ϕ} are tabulated as functions of temperature and average composition, while for each phase ϕ the mass enthalpy, h^{ϕ}, and the density,

ρ^{ϕ}, are tabulated as functions of temperature and phase intrinsic average compositions HERE, as well as other possible parameters. Figure 1 summarizes the steps in order to perform a temperature-to-enthalpy (T2H) conversion using the predefined tabulation approach. In step 1, the transformation path is acquired for each average composition and temperature to determine the list of phases, their volume fractions g^{ϕ} and their intrinsic compositions $\langle w_i \rangle^{\phi}$. In step 2, the phase enthalpy h^{ϕ} and density ρ^{ϕ} are determined by searching for the temperature and the already known phase composition $\langle w_i \rangle^{\phi}$. In step 3, the average volume enthalpy is computed from the volume fraction, density and mass enthalpy of phases using (2.3).

> Figure 3 goes here

The methodology to build the tabulations is straightforward. It is based on two main scans. On the one hand, intervals for the variation of the average composition $\langle w_i \rangle$ are chosen from the known alloy composition. These variations have to cover the extreme values adopted during the simulation, which are not known a priori. An interval is also selected for the variation of temperature. The latter is easier to determine as it usually starts from the initial melt temperature and goes down to the room temperature in a standard casting simulation. For these intervals, a systematic scan is made with chosen steps in each composition and T, during which a thermodynamic equilibrium is computed. The outputs are the number of phases encountered, together with their fraction and intrinsic composition. The minimum and maximum intrinsic composition for each phase could then be determined. On the other hand, for each phase, a scan of the intrinsic composition and temperature is made to compute the intrinsic properties. The same temperature interval and step as defined earlier are used.

> below paragraph should be re written and maybe stress LESS on the speed effect

> I should change the superscript k which may be confused with partition coefficient

Regarding the enthalpy-to-temperature conversion (H2T), a backward iterative T2H search is performed. For a known composition $\langle w_i \rangle$, denoting k the iteration index to convert the enthalpy $\langle \rho h \rangle_{\text{input}}$, we start with an initial guess for temperature $T^{(k=0)}$ then convert it to an enthalpy $\langle \rho h \rangle^{(k=0)}$ with the T2H conversion. Using an appropriate nonlinear algorithm (Brent is the most versatile in our case), we aim at minimizing the following residual: $\text{Residu}_{\langle \rho h \rangle} = \left| \langle \rho h \rangle_{\text{input}} - \langle \rho h \rangle^{(k)} \right|$. Once the algorithm has converged, the temperature $T^{(k)}$ is the result of the H2T conversion. It is inferred that the first conversion (T2H) is a direct one whereas the latter (H2T) is indirect and requires a series of iterative steps; each step being a single T2H resolution. In other words, a H2T conversion is a backward search for a temperature, hence it's slower. This conversion's speed lag is exacerbated when tabulations increase in size (e.g. large number of temperature and composition steps) and complexity (e.g., multicomponent industrial alloys used in casting), since the search gets more complicated with the increasing number of input columns (one column for each alloying element).

2.3 Formulation

> Coming soon

Parameter	Symbol	Value	Unit
Nominal composition	$\langle w \rangle_0$	7	wt.%
Liquidus temperature	T_L	618	°C
Eutectic temperature	T_E	577	°C
Segregation coefficient	k	0.13	–
Liquidus slope	m_L	−6.5	$\mathrm{K\,wt.\%^{-1}}$
Heat capacity (liquid and solid)	ρC_p	2.6×10^6	$\mathrm{J\,m^{-3}\,K^{-1}}$
Enthalpy of fusion	ρL	9.5×10^8	$\mathrm{J\,m^{-3}}$
Thermal conductivity (liquid and solid)	κ	70	$\mathrm{W\,m^{-1}\,K^{-1}}$
Heat transfer coefficient	h_{ext}	500	$\mathrm{W\,m^{-2}\,K^{-1}}$
External temperature	T_{ext}	100	°C
Initial temperature	T_0	800	°C
Ingot length		0.1	m
FE mesh size		10^{-3}	m
Time step	Δt	0.1	s
Convergence criterion (residual)	ε_R	10^{-6}	–
Convergence criterion (temperature)	ε_T	10^{-2}	K

Table 2.1: Parameters for the pure diffusion test case with alloy Al – 7 wt.% Si presented in **FIGURE REF**

2.4 Validation

2.4.1 Pure diffusion

The two solvers are first tested in a purely diffusive case for a one-dimensional solidification configuration. Predictions with a 1D front tracking model [**?**] is used as a benchmark. It provides solutions for the temperature and solid fraction during directional solidification of a 10 cm long Al – 7 wt.% Si ingot. The melt, with initial uniform temperature, is cooled with a heat exchange coefficient (assuming a Fourier boundary condition) from one side, the other side being adiabatic. All values for alloy properties, initial and boundary conditions and numerical parameters are listed in Table 2.1. For this simple test case, we use linear temperature dependence of the intrinsic phase enthalpies, that is $\langle \rho h \rangle^s = \langle \rho C_p \rangle T$ and $\langle \rho h \rangle^l = \langle \rho C_p \rangle T + \rho L$, where $\langle \rho C_p \rangle$ is the heat capacity per unit volume and ρL is the latent heat per unit volume. Values for $\langle \rho C_p \rangle$ and ρL, as well as for the thermal conductivities, $\kappa = \langle \kappa^l \rangle = \langle \kappa^s \rangle$, are taken constant. Moreover, a Gulliver Scheil approximation is used to compute a single temperature – fraction of solid relationship in the absence of macrosegregation. This is done assuming a linear binary phase diagram and thus requires using the properties listed in Table 2.1, i.e. the segregation coefficient, k, the liquidus slope, m_L, the liquidus temperature, T_L, and the eutectic temperature, T_E. **Figure REF** shows the comparison with the Hsolver and Tsolver. The results are found superimposed to the front tacking solution, thus giving validation of the implementation as well as the iterative schemes presented above to solve the energy conservation.

2.4.2 Convection-diffusion with macrosegregation

Conservation equations in **Table 2** are for mass, momentum and chemical species. As for energy, they are presented after the volume averaging technique has been applied [**?**] [**?**]. Moreover, an assumption of a static and non deformable solid phase is made. Consequently, the mechanical model is reduced to the conservation of momentum in the liquid phase. This assumption also yields some other consequences on the mass balance and the liquid momentum conservation. In the latter, a Darcy term is added to take into account the dissipative interfacial stress in the porous-like mushy zone. Its main parameter is the permeability of the mushy zone, K. It is considered isotropic, hence reducing to a scalar which is given by the Carman-Kozeny relation, based on the secondary dendrite arm spacing $\lambda_2 : K = \frac{g^{l3} \lambda_2^2}{180(1-g^l)^2}$. The liquid density being taken constant, its spatial variations as a function of temperature and average composition are still needed to compute thermosolutal convection forces. For that purpose, the Boussinesq approximation $\langle \rho \rangle^l = \rho_{\text{ref}} \left(1 - \beta_T \left(T - T_{\text{ref}} \right) - \beta_{\langle w \rangle^l} \left(\langle w \rangle^l - w_{\text{ref}}^l \right) \right)$ is used, considering the thermal β_T and solutal $\beta_{\langle w \rangle^l}$ expansion coefficients and a reference density, ρ_{ref}, defined at a reference temperature T_{ref} and reference composition w_{ref}^l. Values for the references are taken at the liquidus temperature and the nominal composition of the alloy, $\langle w \rangle_0$ [**?**]. More details about the FE formulation can be found in [**? ?**]. It should be noted that the macroscopic solute diffusion coefficient in the solid phase is neglected in **REF Eq. 15c**.

> in this table I use directly the simplified equations, but this was done only for the article, now I have to go from the full conservation equations and state the hypothesis and methods that i used to reach this simplified form

$$\nabla \cdot \left(g^l \vec{v}^l \right) = 0 \tag{2.4a}$$

$$\frac{\partial}{\partial t} \left(g^l \rho_{\text{ref}} \vec{v}^l \right) + \vec{\nabla} \cdot \left(g^l \rho_{\text{ref}} \vec{v}^l \times \vec{v}^l \right) - \vec{\nabla} \cdot \langle S \rangle^l - g^l \nabla p^l + \mu^l g^{l2} K^{-1} \vec{v}^l - g^l \rho^l \vec{g} = 0 \tag{2.4b}$$

$$\frac{\partial}{\partial t} \left(\langle w_i \rangle \right) + \left(g^l \vec{v}^l \right) \cdot \vec{\nabla} \langle w_i \rangle^l + \nabla \cdot \left(g^l D^l \vec{\nabla} \langle w_i \rangle^l \right) = 0 \tag{2.4c}$$

Table 2.2: Averaged conservation equations for the conservation of mass (a), momentum (b) and solute mass (c)

> Figure SMACS: Computed unidirectional heat diffusion during solidification of an Al – 7 wt.% Si alloy using (orange) the enthalpy method and (black) the temperature method, comparison being made for (left) cooling curves and (right) time history of the liquid fraction. Each curve corresponds to a position along the sample, from 0 cm (cooling side) to 10 cm (insulated side), with 2 cm spacing between the positions.

The Tsolver's ability to be coupled with various physical phenomena like macrosegregation and fluid flow in porous medium is displayed in this test case. It consists of a solidification benchmark where a 10 cm width × 6 cm height × 1 cm thick cavity containing a Sn – 3 wt.% Pb melt is cooled down from its two narrowest vertical sides using heat exchangers (LHE: left heat exchanger, RHE: right heat exchanger). The experiment, inspired by Hebditch and

Hunt's [**?**] similar set up, has been revisited by Hachani et al. [**?**] who performed the solidification with better controlled conditions and using an increased number of samples for composition analysis. Recently, a successful attempt to simulate the experiment was carried out by Carozzani et al. relying on an enthalpy resolution [**?**]. All details regarding geometry, finite element discretization, material properties and boundary conditions can be found in the latter reference.

I could develop more here giving additional details

For this computation, solidification paths, phase compositions and phase enthalpies were determined by a thermodynamic module dedicated to equilibrium calculations for binary alloys. The 3D simulation results in **REF Figure 4** show a satisfactory agreement with the experimental temperature measurements recorded at mid heights of the cavity and uniformly distributed along its width [**?**]. In fact, simulation results with the Tsolver and the Hsolver were found to be almost superimposed, as in **REF Figure 4**. Regarding the computation, the Tsolver resolution proves to be faster than the Hsolver used in [**?**]: a process time of 7000s required a computation time of 90 hours 13 minutes compared to 114 hours 21 minutes spent by the enthalpy resolution with 32 cores on the same cluster. The gain factor is about 20%.

Chapter 3

Macrosegregation without solidification shrinkage

Contents

this chapter discusses the following points:

- General introduction about freckles

- Couling the energy resolution from chapter 2 to fluid mechanics and solute balance

- Application: Ternary solidification with freckles

- Application: Macroscopic Freckle predicition: pure FE

- Application Multiscale Freckle predicition: FE + grain structure (in which lies a part about nucleation-growth and how numerically we reach a smaller scale, the scale of the grain boundaries)

3.1   Application to multicomponent alloys

The efficiency of the temperature-based resolution resides in its performance when combined with thermodynamic tabulations. A multicomponent alloy consists of at least two solute elements, and therefore the tabulation size increases, hence the number of search operations also increases. To demonstrate the speed-up ability of the temperature-based approach while predicting all phase transformations during macrosegregation, we consider the solidification of a ternary alloy, Fe–2 wt.%C– 30 wt.%Cr. As illustrated in **Figure 5a**, the alloy domain has a cylinder shape close to 3-inch height × 1-inch diameter. Exact values are reported in **Table 3** with all material properties, initial and boundary conditions, as well as numerical parameters for the simulations. The melt steel is initially at 1395 °C. The temperature of the bottom surface is imposed with a constant decreasing rate of 0.1 K.s-1 starting with 1380 °C, i.e. 40 °C higher than the nominal liquidus temperature, as shown in **Figure 5b**. The other surfaces are kept adiabatic. The cylinder is held in a vertical position. In these conditions, and knowing that the carbon and chromium solutes have lightening effects on the liquid at nominal composition, the density inversion resulting from the composition gradient in the interdendritic liquid, may cause flow instability (segregation plumes) at the solidification front. While the selected alloy is a steel, this application is also representative of directional cooling in a single crystal casting, e.g. for nickel-base superalloys [**?**]. **Figure 5c** also provides the transformation path of the alloy at nominal composition, i.e. assuming no macrosegregation and full thermodynamic equilibrium as computed with ThermoCalc and the TCFE6 database [**? ?**]. A total of 5 phases need to be handled, the characteristic temperature for their formation being reported in **Figure 5b**.

Figure 5: Configurations for directional casting of (a) a 1 inch diameter × 3 inches height cylindrical domain for which (b) temperature-time conditions are imposed at its bottom surface. The alloy is Fe – 2 wt.% C– 30 wt.% Cr, its computed transformation path [20], [21] at nominal composition being displayed in (c)

3.1.1   Tabulations

Full thermodynamic equilibrium is considered in the present case. Due to macrosegregation, the average composition is expected to continuously vary in time and space during casting.

Transformation paths are thus determined a priori for a set of average compositions around the nominal value. Hence, carbon content is arbitrarily varied in the interval [1.8 wt.%, 2.2 wt.%] while chromium content variation is in the interval [27 wt.%, 33 wt.%]. The offset of ±10% with respect to the nominal composition value allows tabulating relatively small composition steps to ensure a good accuracy when compared to the corresponding ternary phase diagram. The average composition step is -0.04wt.% for carbon and -0.6wt.% for chromium, thus representing 2% intervals with respect to the nominal composition. The temperature varies in the interval [100 °C,1600 °C] by 5 °C steps. For each triplet (carbon content in wt.% C, **HERE** , chromium content in wt.% Cr, **HERE**, temperature in K) corresponds a phase fraction g^ϕ and a pair of intrinsic phase composition (**HERE**). For the 5 phases listed in **Figure 5c** (LIQ≡liquid, BCC≡ferrite, FCC≡austenite, M_7C_3 ≡carbide, CEM≡cementite), the enthalpy h^ϕ and density ρ^ϕ, are tabulated as functions of temperature and phase intrinsic composition. If this latter input lies between two tabulated values, a linear interpolation is performed to determine the output, i.e. phase enthalpy and density. With the advancement of solidification, the liquid is enriched with solute by macrosegregation, which enables new solidification paths. It means that the primary solidifying phase is not necessarily the same as when considering the nominal composition. For this reason, the tabulation approach is interesting inasmuch as it provides phase transformation paths and values of phase properties that are compatible with the system's actual composition. **Figure 6** summarizes the tabulated thermodynamic data for two sets of average composition for the considered ternary system. Note that in the present test case, phase densities are taken constant ($\rho^s = \rho^l = 6725 \, \mathrm{kg\,m}^{-3}$). Therefore they are not tabulated. With this assumption, no shrinkage occurs upon phase change.

Parameter	Symbol	Value	Unit
Nominal composition	$\langle w_C \rangle_0$	2	wt.%
	$\langle w_{Cr} \rangle_0$	30	wt.%
Characteristic temperatures	T_{top}, T_{bottom}	**FIGURE**	°C
Phase fraction	g^{ϕ}	Tabulations	–
Phase enthalpy	$\langle h \rangle^{\phi}$	Tabulations	–
Phase composition	$\langle w_C \rangle^{\phi}$	Tabulations	wt.%
	$\langle w_{Cr} \rangle^{\phi}$	Tabulations	wt.%
Diffusion coefficients	$\langle D_C \rangle^l$	15×10^{-10}	$m^2\,s^{-1}$
	$\langle D_{Cr} \rangle^l$	15×10^{-10}	$m^2\,s^{-1}$
Dynamic viscosity	μ^l	2×10^{-3}	Pa s
Thermal expansion coefficient	β_T	8.96×10^{-5}	K^{-1}
Solutal expansion coefficient	$\beta_{\langle w_C \rangle^l}$	1.54×10^{-3}	wt.%$^{-1}$
	$\beta_{\langle w_{Cr} \rangle^l}$	1.72×10^{-2}	wt.%$^{-1}$
Thermal conductivity in the solid	$\langle \kappa^s \rangle$	40	$W\,m^{-1}\,K^{-1}$
Thermal conductivity in the liquid	$\langle \kappa^l \rangle$	28	$W\,m^{-1}\,K^{-1}$
Dendrite arm spacing	λ	60×10^{-6}	m
Density	ρ_{ref}	6725	$kg\,m^{-3}$
Initial temperature	T_0	1395	°C
Ingot diameter		25×10^{-3}	m
Ingot length		75×10^{-3}	m
FE mesh size		10^{-3}	m
Time step	Δt	0.1	s
Convergence criterion (residual)	ε_R	10^{-6}	–
Convergence criterion (temperature)	ε_T	10^{-2}	K

Table 3.1: Parameters for solidification of alloy Fe – 2 wt.% C – 30 wt.% Cr

Chapter 4

Macrosegregation with solidification shrinkage

Contents

this chapter discusses the following points:

- Density variation during solidification (industrial point of view then how to handle numerically)

- Model equations

- Application to solidification benchmark SMACS

- Possible extension of application with grain structure (using Shijia's LS-air cells handling)

- Multiscale Freckle predicition: FE + grain structure (in which lies a part about nucleation-growth and how numerically we reach a smaller scale, the scale of the grain boundaries)

4.1 Introduction

Solidification shrinkage is, by definition, the effect of relative density change between the liquid and solid phases. In general, it results in a progressive volume change during solidification, until the phase change has finished. Figure 4.1. The four stages Figure 4.1a, **??**, **??** and **??** depict the volume change with respect to solidification time. First, at the level of the first solid crust, near the local solidus temperature, the solid forms with a density smaller than the liquid's. This does not necessarily apply for all materials, but at least for steels it does. The subsequent volume difference tends to create voids with a big negative pressure, that needs to be compensated by a surrounding fluid. It thus drains the liquid metal in its direction (cf. Figure 4.1b). As a direct result of the inward feeding flow, the ingot surface tends to gradually deform in the feeding direction, forming the so-called *shrinkage pipe*. Since the mass of the alloy and its chemical species are conserved, a density difference between the phases ($\rho^s > \rho^l$), leads to a different overall volume ($V^s < V^l$), once solidification is complete, as confirm the following equations:

$$\rho^l V^l = \rho^s V^s \tag{4.1a}$$

$$V^s = \frac{\rho^l}{\rho^s} V^l \tag{4.1b}$$

4.2 Mass Conservation

4.2.1 Assumptions

- Two phases are considered, liquid l and solid s: $g^l + g^s = 1 \implies \frac{dg^l}{dt} = -\frac{dg^s}{dt}$

- The phase densities are constant but not equal: $\rho^l = cst_1$ and $\rho^s = cst_2$. Thermal and solutal expansion/contraction is neglected

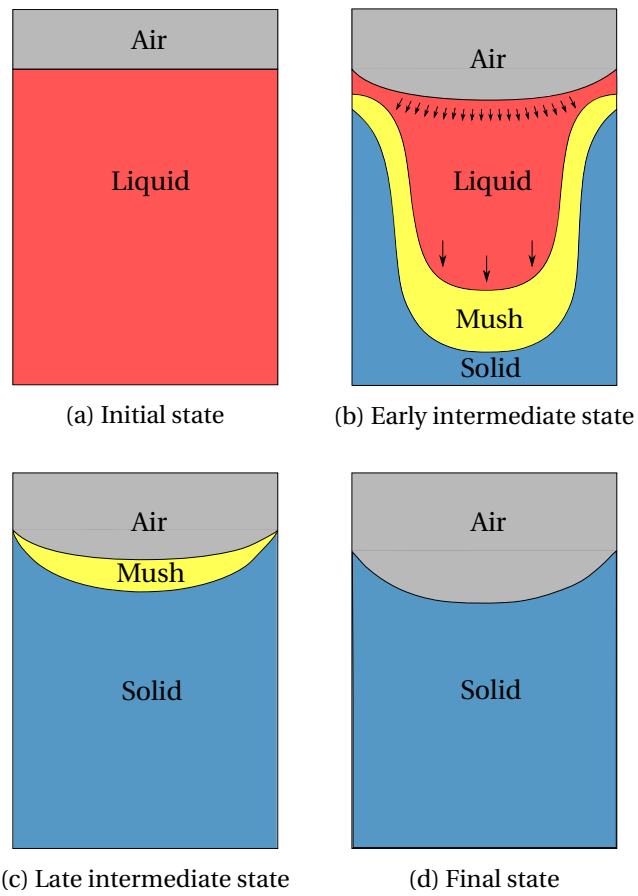- The solid phase is assumed static: $\vec{v^s} = \vec{0}$, which yields the following consequences:

Figure 4.1: Schematic of the main cooling stages of an ingot against side and bottom mould walls (not shown)

1. $\langle \vec{v} \rangle = g^l \vec{v^l} + g^s \vec{v^s}^{\,\,0} = g^l \vec{v}^l$

2. $\langle \rho \vec{v} \rangle = g^l \rho^l \vec{v}^l + g^s \rho^l \vec{v^s}^{\,\,0} = g^l \rho^l \vec{v}^l$

3. $\dfrac{\partial \rho^l}{\partial t} = \dfrac{\partial \rho^s}{\partial t} = 0$

4. $\vec{\nabla} \rho^l = \vec{\nabla} \rho^s = \vec{0}$

4.2.2 Formulation

The mass balance equation averaged over the two phases, is developed taking into account the assumptions made earlier.

$$\frac{\partial \langle \rho \rangle}{\partial t} + \nabla \cdot \langle \rho \vec{v} \rangle = 0 \tag{4.2a}$$

$$\frac{\partial}{\partial t}\left(g^l \rho^l + g^s \rho^s \right) + \nabla \cdot \left(g^l \rho^l \vec{v}^l \right) = 0 \tag{4.2b}$$

$$g^l \frac{\partial \rho^l}{\partial t} + \rho^l \frac{\partial g^l}{\partial t} + g^s \frac{\partial \rho^s}{\partial t} + \rho^s \frac{\partial g^s}{\partial t} + \rho^l \nabla \cdot \left(g^l \vec{v}^l \right) + g^l \vec{v}^l \cdot \vec{\nabla} \rho^l = 0 \tag{4.2c}$$

$$\left(\rho^l - \rho^s \right) \frac{\partial g^l}{\partial t} + \rho^l \nabla \cdot \left(g^l \vec{v}^l \right) = 0 \tag{4.2d}$$

$$\boxed{\nabla \cdot \left(g^l \vec{v}^l \right) = \nabla \cdot \langle \vec{v}^l \rangle = \frac{\rho^l - \rho^s}{\rho^l} \frac{\partial g^s}{\partial t}} \tag{4.3}$$

4.2.3 Discussion

With the assumptions of static solid phase and constant unequal phase densities, the average mass balance states that the divergence of the liquid velocity is proportional to the solidification rate, the proportionality constant being the relative density change (which results in a relative volume change). This relation between the liquid velocity and the temporal derivative of the solid fraction, explains the flow due to shrinkage. In metallic alloys, the solid density is usually greater than the liquid density, therefore the first term in the RHS is negative. As for the second term, if we neglect remelting, then it'll be positive in the solidifying areas of the alloy. A negative divergence term in these areas, means that a liquid feeding is necessary to compensate for the density difference, hence acting as a flow driving force in the melt. In the case of constant densities, we can easily deduce that the divergence term is null, and therefore no flow is induced by solidification.

Numerically speaking, a non-zero divergence term in the mass balance is equivalent to a compressible fluid behaviour. Additional terms should appear in the other conservation equations, balancing the volume change in the momentum, heat and species transport.

4.3 Momentum Conservation

In a typical volume averaging approach, one would write one momentum conservation equation for each phase. Nonetheless, only one equation will be present in our case, and that is the consequence of the assumption of the static solid, made in the previous section. It should be emphasized that, despite considering a single conservation equation, the effect of the solid movement with respect to the liquid's can still be incorporated through the interfacial fluxes in the momentum conservation of the liquid phase.

4.3.1 Assumptions

- The interfacial momentum transfer between the solid and liquid phases is modelled by a momentum flux vector $\vec{\Gamma}^l$, consisting of hydrostatic and deviatoric parts, such that:

$$\vec{\Gamma}^l = \vec{\Gamma}^l_p + \vec{\Gamma}^l_{\mathbb{S}} \tag{4.4a}$$

$$\vec{\Gamma}^l_p = p^{l^*}\vec{\nabla}g^l = p^l\vec{\nabla}g^l \tag{4.4b}$$

$$\vec{\Gamma}^l_{\mathbb{S}} = -g^{l2}\mu^l\mathbb{K}^{-1}\left(\vec{v}^l - \vec{v}^s\right) \tag{4.4c}$$

where p^{l^*} is the pressure at the interface, considered to be equal to the liquid hydrostatic pressure, $\mathbb{K}$ is the permeability computed by the Carman-Kozeny relation and μ^l is the liquid's dynamic viscosity. For the solid phase, the interfacial terms are the opposite, which cancels them out with the liquid terms if the phase momentum equations are summed up.

- The liquid is considered as a *compressible* Newtonian fluid. It implies that the deviatoric part, $\mathbb{S}^l$, of the Cauchy stress tensor is decomposed as follows:

> CAG: the liquid is incompressible, but the mixture is compressible, change it

$$\langle\underline{\sigma}^l\rangle = -\langle p^l\rangle\underline{\mathbb{I}} + \langle\underline{\mathbb{S}}^l\rangle \tag{4.5a}$$

$$\langle\underline{\sigma}^l\rangle = -\langle p^l\rangle\underline{\mathbb{I}} + 2\mu^l\langle\underline{\dot{\varepsilon}}^l\rangle + \langle\underline{\tau}^l\rangle \tag{4.5b}$$

where $\langle\underline{\dot{\varepsilon}}^l\rangle$ is the strain rate tensor that depends on the average liquid velocity:

$$\langle\underline{\dot{\varepsilon}}^l\rangle = \underline{\nabla}\langle\vec{v}^l\rangle + \underline{\nabla}^{\mathbf{t}}\langle\vec{v}^l\rangle \tag{4.6}$$

and $\underline{\tau}^l$ is the extra stress tensor in the liquid, given by:

$$\langle\underline{\tau}^l\rangle = -\lambda\nabla\cdot\langle\vec{v}^l\rangle\underline{\mathbb{I}} \tag{4.7a}$$

where λ is a dilatational viscosity **CITE RAP2003**. For an incompressible flow, the divergence term vanishes, hence the classical Newtonian constitutive law is retrieved. In the literature, the coefficient λ is taken proportional to the viscosity: $\lambda = \frac{2}{3}\mu^l$

4.3.2 Formulation

The momentum conservation equation in the liquid writes:

$$\frac{\partial}{\partial t}\left(\rho^l g^l \vec{v}^l\right) + \vec{\nabla}\cdot\left(\rho^l g^l \vec{v}^l \times \vec{v}^l\right) = \vec{\nabla}\cdot\left(g^l \underline{\sigma}^l\right) + g^l \vec{F}_{\rm V} + \vec{\Gamma}^l \tag{4.8}$$

where $\vec{F}_{\rm v}$ is an external volume force. The effect of the mass balance obtained in the previous section is incorporated by expanding the temporal and spatial derivatives in the momentum equation, taking firstly the left-hand side of equation (4.8).

$$\text{LHS} = \rho^l \frac{\partial}{\partial t}\left(g^l \vec{v}^l\right) + g^l \vec{v}^l \cancel{\frac{\partial\rho}{\partial t}} + \vec{v}^l \nabla\cdot\left(\rho^l g^l \vec{v}^l\right) + \underline{\nabla}\vec{v}^l\left(\rho^l g^l \vec{v}^l\right) \tag{4.9a}$$

$$= \rho^l \underbrace{\frac{\partial}{\partial t}\left(g^l \vec{v}^l\right)}_{\substack{\text{Unsteady}\\\text{Acceleration}}} + \left(\rho^l - \rho^s\right)\underbrace{\frac{\partial g^s}{\partial t}\vec{v}^l}_{\substack{\text{Shrinkage}\\\text{Acceleration}}} + \rho^l \underbrace{\underline{\nabla}\vec{v}^l\left(g^l \vec{v}^l\right)}_{\substack{\text{Advective}\\\text{Acceleration}}} \tag{4.9b}$$

The development in (4.9b) shows that the origin of the flow, namely its acceleration, is attributed to three causes: i) unsteady acceleration: a temporal change of a particle's velocity, ii) shrinkage-induced acceleration: a local "suction" effect at the solid-liquid interface (where $\frac{\partial g^s}{\partial t} > 0$) caused by the density jump $\left(\rho^l - \rho^s\right)$ and iii) convective acceleration: a spatial change in the velocity field. The effect of the *shrinkage-induced* flow is introduced using the mass balance in equation (4.3). The right-hand side of equation (4.8) is now expanded:

$$\text{RHS} = \vec{\nabla}\cdot\left(\langle p^l\rangle\underline{\mathbb{I}} + 2\mu^l\langle\underline{\dot{\varepsilon}}^l\rangle + \langle\underline{\tau}^l\rangle\right) + g^l \rho^l \vec{g} + \vec{\Gamma}^l_p + \vec{\Gamma}^l_{\mathbb{S}} \tag{4.10a}$$

$$= -\vec{\nabla}\left(g^l p^l\right) + \vec{\nabla}\cdot\left(2\mu^l\langle\underline{\dot{\varepsilon}}^l\rangle\right) + \vec{\nabla}\cdot\left(-\frac{2}{3}\mu^l\nabla\cdot\langle\vec{v}^l\rangle\underline{\mathbb{I}}\right) + g^l\rho^l\vec{g} + \vec{\Gamma}^l_p + \vec{\Gamma}^l_{\mathbb{S}} \tag{4.10b}$$

$$= \cancel{-p^l\vec{\nabla}g^l} - g^l\vec{\nabla}p^l + \vec{\nabla}\cdot\left(2\mu^l\langle\underline{\dot{\varepsilon}}^l\rangle\right) + \vec{\nabla}\cdot\left(-\frac{2}{3}\mu^l\nabla\cdot\langle\vec{v}^l\rangle\underline{\mathbb{I}}\right) + g^l\rho^l\vec{g} + \cancel{\vec{\Gamma}^l_p} + \vec{\Gamma}^l_{\mathbb{S}} \tag{4.10c}$$

$$= -g^l\vec{\nabla}p^l + \vec{\nabla}\cdot\left(\mu^l\left(\underline{\nabla}\langle\vec{v}^l\rangle + {}^{\mathbf{t}}\underline{\nabla}\langle\vec{v}^l\rangle\right)\right) + \vec{\nabla}\cdot\left(-\frac{2}{3}\mu^l\frac{\rho^l - \rho^s}{\rho^l}\frac{\partial g^s}{\partial t}\right) + g^l\rho^l\vec{g} - g^{l^2}\mu^l\mathbb{K}^{-1}\vec{v}^l \tag{4.10d}$$

The system thus consists of 3 equations (one for each of the components of $\vec{v}^l$) and 4 unknowns ($\vec{v}^l_x$, $\vec{v}^l_y$, $\vec{v}^l_z$ and p). An additional equation is provided by the mass continuity equation (4.3). For convenience, the superficial velocity $\langle\vec{v}^l\rangle$ will be chosen as a velocity unknown instead of the intrinsic average: $\langle\vec{v}^l\rangle = g^l\vec{v}^l$. The final system to solve, after grouping the unknowns in the LHS and the remaining terms in the RHS, is given by:

> I changed *split* to *align* here

$$\rho^l \frac{\partial \langle \vec{v}^l \rangle}{\partial t} + \frac{\rho^l - \rho^s}{g^l} \frac{\partial g^s}{\partial t} \langle \vec{v}^l \rangle + \rho^l \underline{\nabla} \vec{v}^l \langle \vec{v}^l \rangle + \vec{\nabla} \cdot \left(2\mu^l \langle \underline{\dot{\varepsilon}}^l \rangle \right) + g^l \mu^l \mathbb{K}^{-1} \langle \vec{v}^l \rangle \tag{4.11}$$

$$= g^l \vec{\nabla} p^l + \vec{\nabla} \left(-\frac{2}{3} \mu^l \nabla \cdot \langle \vec{v}^l \rangle \right) + g^l \rho^l \vec{g} \tag{4.12}$$

$$\nabla \cdot \langle \vec{v}^l \rangle = \frac{\rho^l - \rho^s}{\rho^l} \frac{\partial g^s}{\partial t} \tag{4.13}$$

4.4 Energy Conservation

We have seen the averaged energy conservation equation in the case of two phases: a solid phase and an incompressible liquid phase. However, with the incorporation of the shrinkage effect, new terms should appear in the advective-diffusive heat transfer equation.

4.4.1 Assumptions

- The thermal conductivity is constant for both phases: $\langle \kappa \rangle = \langle \kappa^s \rangle = \langle \kappa^l \rangle = \kappa$

- Consequence of the static solid phase: $\langle \rho h \vec{v} \rangle = g^l \rho^l h^l \vec{v}^l + \cancel{g^s \rho^s h^s \vec{v}^s} = g^l \rho^l h^l \vec{v}^l$

- The system's enthalpy may thermodynamically evolve with pressure, knowing that $h = e + \frac{p}{\rho}$, where e is the internal energy and p is the pressure. It infers that the heat transport equation may contain a contribution attributed to volume compression/expansion:

$$\frac{\partial p}{\partial t} + \nabla \cdot \left(p \vec{v} \right) = \frac{\partial p}{\partial t} + p \nabla \cdot \vec{v} + \vec{v} \cdot \vec{\nabla} p \tag{4.14}$$

In the literature, this contribution has been always neglected, even when accounting for solidification shrinkage, owing to the small variations of pressure.

- Another contribution is also neglected in solidification problems, that is the heat generated by mechanical deformation, $\mathbb{S} : \dot{\varepsilon}$

4.4.2 Formulation

The unknowns in the energy conservation are the average volumetric enthalpy $\langle \rho h \rangle$ and temperature T. The energy conservation equation writes:

$$\frac{\partial \langle \rho h \rangle}{\partial t} + \nabla \cdot \langle \rho h \vec{v} \rangle = \nabla \cdot \left(\langle \kappa \rangle \vec{\nabla} T \right) \tag{4.15a}$$

$$\frac{\partial \langle \rho h \rangle}{\partial t} + \nabla \cdot \left(g^l \rho^l h^l \vec{v}^l \right) = \nabla \cdot \left(\kappa \vec{\nabla} T \right) \tag{4.15b}$$

$$\frac{\partial \langle \rho h \rangle}{\partial t} + \rho^l h^l \nabla \cdot \langle \vec{v}^l \rangle + \langle \vec{v}^l \rangle \cdot \vec{\nabla} \left(\rho^l h^l \right) = \nabla \cdot \left(\kappa \vec{\nabla} T \right) \tag{4.15c}$$

$$\frac{\partial \langle \rho h \rangle}{\partial t} + \cancel{\rho^l} h^l \frac{\rho^l - \rho^s}{\cancel{\rho^l}} \frac{\partial g^s}{\partial t} + \langle \vec{v}^l \rangle \cdot \vec{\nabla} \left(\rho^l h^l \right) = \nabla \cdot \left(\kappa \vec{\nabla} T \right) \tag{4.15d}$$

$$\frac{\partial \langle \rho h \rangle}{\partial t} + \left(\rho^l - \rho^s \right) h^l \frac{\partial g^s}{\partial t} + \langle \vec{v}^l \rangle \cdot \vec{\nabla} \left(\rho^l h^l \right) = \nabla \cdot \left(\kappa \vec{\nabla} T \right) \tag{4.15e}$$

$$\boxed{\frac{\partial \langle \rho h \rangle}{\partial t} + \rho^l \langle \vec{v}^l \rangle \cdot \vec{\nabla} h^l = \nabla \cdot \left(\kappa \vec{\nabla} T \right) + \left(\rho^s - \rho^l \right) h^l \frac{\partial g^s}{\partial t}} \tag{4.16}$$

4.4.3 Discussion

In order to keep things simple, the term "enthalpy" will refer henceforth to "volume enthalpy", otherwise, we will explicitly use the term "mass enthalpy". It is important to understand the meaning of the terms in equation (4.16). The first term in the left-hand side is the temporal change in the system's average enthalpy, i.e. a temporal change in the volume enthalpy of any of the phases in the course of solidification. The second LHS term is a dot product between the superficial liquid velocity and the the gradient of the liquid's enthalpy. Since phase densities are constant in our case, the gradient term reduces to the liquid's mass enthalpy. If we consider a representative volume element (RVE) in the liquid phase, far from the mushy zone, we can stipulate:

$$\vec{\nabla} h^l = C_p^l \vec{\nabla} T \tag{4.17}$$

assuming that the phase mass specific heat, C_p^l, is constant. Therefore, the liquid enthalpy is advected in the case where the velocity vector is not orthogonal to the temperatre gradient. The advection reaches its maximum when the two vectors have the same direction. Consider, for instance, a filled ingot with a cooling flux applied to its bottom surface. If the density variation with temperature were to be neglected, then the sole mechanical driving force in the melt is the density jump at the solid-liquid interface ahead of the mushy zone. The temperature gradient in such a case is vertical upward, while the velocity vector is in the opposite direction. The advective term writes:

$$\rho^l \langle \vec{v}^l \rangle \cdot \vec{\nabla} h^l = -\rho^l C_p^l \| \langle \vec{v}^l \rangle \| \| \vec{\nabla} T \| \tag{4.18}$$
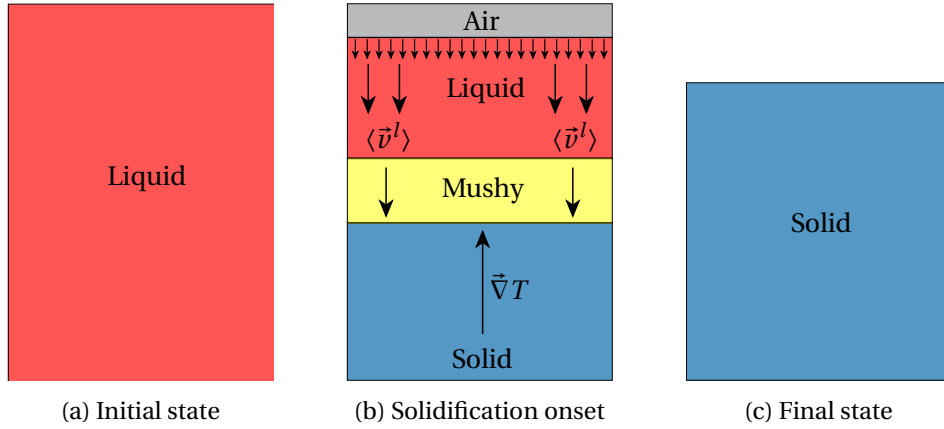
Figure 4.2: Effect of shrinkage flow on a solidifying ingot

We see that the second RHS term in equation (4.16) acts as a heat source at the interface between the the phases, in this particular solidification scenario. Another heat power (of unit Wm^{-3}) adds to the system within the mushy, that is the second term in the right-hand side of the same equation. This term is proportional to the solidification rate. Finally, the first RHS term accounts for thermal diffusion within the phases.

It should be emphasized that the assumption of a constant specific heat in the liquid in equation (4.17) applies when no macrosegregation occurs. Nonetheless, when the latter is considered, the phases specific and latent heats become highly dependent on the local average composition. It then advisable to use the thermodynamic tabulation approach, where the enthalpies are directly tabulated as functions of temperature and composition.

4.5 Species Conservation

The last conservation principle is applied to the chemical species or solutes. This principle allows predicting macrosegregation when applied to a solidification system, along with the mass, momentum and energy balances. However, the conservation equation should be reformulated in the case of a melt flow driven by shrinkage.

4.5.1 Assumptions

- The alloy is binary, i.e., it is composed from one solute, and hence the notation of the average composition without a solute index: $\langle w \rangle$ for the mass composition and $\langle \rho w \rangle$ for the volume composition

- The solid fration is determined assuming complete mixing in both phases, hence the lever rule is applicable. It should be mentionned that the solidification path in the current approach is tabulated using thermodynamic data at equilibrium

- The solutal diffusion coefficient D^s in the solid phase is neglected in the mass diffusive flux term. The remaining term, D^l, is a mass diffusion coefficient in the liquid phase, of

unit $m^2 s^{-1}$

- Consequence of the static solid phase: $\langle \rho w \vec{v} \rangle = g^l \rho^l \langle w \rangle^l \vec{v}^l + \cancel{g^s \rho^s \langle w \rangle^s \vec{v}^s} = g^l \rho^l \langle w \rangle^l \vec{v}^l$

4.5.2 Formulation

The species conservation is pretty similar the energy conservation formluted in the previous section. For a binary alloy, we can write:

$$\frac{\partial \langle \rho w \rangle}{\partial t} + \nabla \cdot \langle \rho w \vec{v} \rangle = \nabla \cdot \left(\rho^l \langle D^l \rangle \vec{\nabla} \langle w \rangle^l \right) \tag{4.19a}$$

$$\frac{\partial \langle \rho w \rangle}{\partial t} + \nabla \cdot \left(g^l \rho^l \langle w \rangle^l \vec{v}^l \right) = \nabla \cdot \left(g^l \rho^l D^l \nabla \langle w \rangle^l \right) \tag{4.19b}$$

$$\frac{\partial \langle \rho w \rangle}{\partial t} + \rho^l \langle w \rangle^l \nabla \cdot \langle \vec{v}^l \rangle + \langle \vec{v}^l \rangle \cdot \vec{\nabla} \left(\rho^l \langle w \rangle^l \right) = \nabla \cdot \left(g^l \rho^l D^l \vec{\nabla} \langle w \rangle^l \right) \tag{4.19c}$$

$$\frac{\partial \langle \rho w \rangle}{\partial t} + \cancel{\rho^l} \langle w \rangle^l \frac{\rho^l - \rho^s}{\cancel{\rho^l}} \frac{\partial g^s}{\partial t} + \langle \vec{v}^l \rangle \cdot \vec{\nabla} \left(\rho^l \langle w \rangle^l \right) = \nabla \cdot \left(g^l \rho^l D^l \vec{\nabla} \langle w \rangle^l \right) \tag{4.19d}$$

$$\frac{\partial \langle \rho w \rangle}{\partial t} + \left(\rho^l - \rho^s \right) \langle w \rangle^l \frac{\partial g^s}{\partial t} + \langle \vec{v}^l \rangle \cdot \vec{\nabla} \left(\rho^l \langle w \rangle^l \right) = \nabla \cdot \left(g^l \rho^l D^l \vec{\nabla} \langle w \rangle^l \right) \tag{4.19e}$$

$$\boxed{\frac{\partial \langle \rho w \rangle}{\partial t} + \rho^l \langle \vec{v}^l \rangle \cdot \vec{\nabla} \langle w \rangle^l = \nabla \cdot \left(\rho^l D^l \vec{\nabla} \langle w \rangle^l \right) + \left(\rho^s - \rho^l \right) \langle w \rangle^l \frac{\partial g^s}{\partial t}} \tag{4.20}$$

4.5.3 Discussion

The species transport equation is usually derived with the volumetric average composition $\langle \rho w \rangle$, then divided by the density, which is constant if no solidification shrinkage occurs. In the case where macrosegregation is solely due to fluid flow generated by natural or forced convection, the overall volume remains constant. It is thus convenient to compute composition variations using the mass variable $\langle w \rangle$. However, in the current context, the volume is subject to changes, hence the formulation of equation (4.20) with $\langle \rho w \rangle$.

Chapter 5

Macrosegregation with shrinkage and deformable solid OR Application to TEXUS

This chapter will depend on the progress in the shrinkage simulations. If everything goes with shrinkage, then maybe i can put it in Thercast and test the solid deformation also and apply to TEXUS If not then this chapter will only cover these topics:

- What are the CCEMLCC experimental facilities (ground experiments, sound rocket, ISS)

- Focus on TEXUS (setup, conditions, previous results, recent failures...)

-

Conclusion and Perspectives

Conclusions

The summary of what we did in the previous chapters

Future Work

What did we miss in our models that can be potentialy important for the coming years

Appendicitis A

Notes

from

For many natural-convection flows, you can get faster convergence with the Boussinesq model than you can get by setting up the problem with fluid density as a function of temperature. This model treats density as a constant value in all solved equations, except for the buoyancy term in the momentum equation:

$$(\rho - \rho_0)g \approx -\rho_0 \beta(T - T_0)g \tag{A.1}$$

where ρ_0 is the (constant) density of the flow, T_0 is the operating temperature, and β is the thermal expansion coefficient. Equation 13.2-18 is obtained by using the Boussinesq approximation $\rho = \rho_0(1 - \beta\Delta T)$ to eliminate ρ from the buoyancy term. This approximation is accurate as long as changes in actual density are small; specifically, the Boussinesq approximation is valid when $\beta(T - T_0) \ll 1$.